



CHORUS

This is the accepted manuscript made available via CHORUS. The article has been published as:

Ab Initio Electronic Properties of Monolayer Phosphorus Nanowires in Silicon

D. W. Drumm, J. S. Smith, M. C. Per, A. Budi, L. C. L. Hollenberg, and S. P. Russo

Phys. Rev. Lett. **110**, 126802 — Published 20 March 2013

DOI: [10.1103/PhysRevLett.110.126802](https://doi.org/10.1103/PhysRevLett.110.126802)

Ab initio electronic properties of monolayer phosphorus nanowires in silicon

D. W. Drumm,^{1,2,*} J. S. Smith,² M. C. Per,^{2,3} A. Budi,¹ L. C. L. Hollenberg,¹ and S. P. Russo²

¹*School of Physics, The University of Melbourne, Parkville VIC 3010, Australia*

²*Applied Physics, School of Applied Sciences, RMIT University, Melbourne VIC 3001, Australia*

³*Virtual Nanoscience Laboratory, CSIRO Materials Science and Engineering, Parkville VIC 3052, Australia*

Epitaxial circuitry offers a revolution in silicon technology, with components that can be fabricated on atomic scales. We perform the first *ab initio* calculation of atomically thin epitaxial nanowires in silicon, investigating the fundamental electronic properties of wires two P atoms thick, similar to those produced this year by Weber *et al.* For the first time, we catch a glimpse of disorder-related effects in the wires – a prerequisite for understanding real fabricated systems. Inter-wire interactions are made negligible by including 40 monolayers of silicon in the vertical direction (and the equivalent horizontally). Accurate pictures of band splittings and the electronic density are presented, and for the first time the effective masses of electrons in such device components are calculated.

PACS numbers: 85.35.Be, 73.21.Hb, 85.30.De

After decades of relentless miniaturization, nanoelectronic devices fabricated epitaxially, atom by atom, have given us a glimpse of the end of Moore’s Law for silicon nanoelectronics. Epitaxially doped circuitry fabricated via the STM lithography technique [1] offers atomically-precise control of donors [2, 3], and has improved steadily over the past decade, from basic devices [4, 5] through specialized nanodots [6] and nanowires [7], to a seven-donor quantum dot [8], all doped into a single monolayer. Recent advances include a single-atom transistor [9] and high-conductance nanowires just a few atoms wide [10]. Although single-donor physics is well-known, and that of 2D devices relatively so, in the intermediate nanowire regime *ab initio* understanding (essential to guide multi-scale device modeling) is lacking. The realization of nanocircuitry confined to atomic dimensions both vertically and laterally is of much interest to the spintronics [11, 12] and quantum information processing [13–15] communities.

Theoretical descriptions of these epitaxial systems have improved, with descriptions of infinite δ -doped layers using effective mass theory (EMT) [16], planar Wannier orbitals [17], tight-binding (TB) [18, 19], and *ab initio* density functional theory (DFT) [20–22]. All of these, however, focus on two-dimensional layers without further patterning (although some consider quasi-disorder via the supercell approximation [20, 21]). EMT [8] and self-consistent TB (scTB) [10] are the forefront of device modeling efforts. To date, *ab initio* treatments – an important base for higher-scale and effective methods – have not been able to handle the relatively large volumes involved in such structures.

This intermediate regime, combining high-density doping (with all its accompanying many-body physics), dual confinement directions, and the large Bohr radius of P donors in Si, presents several barriers to modeling efforts. One of the most critical aspects of device design at the atomic scale is knowledge of the effective electronic width, which can be quite different to the lithographic

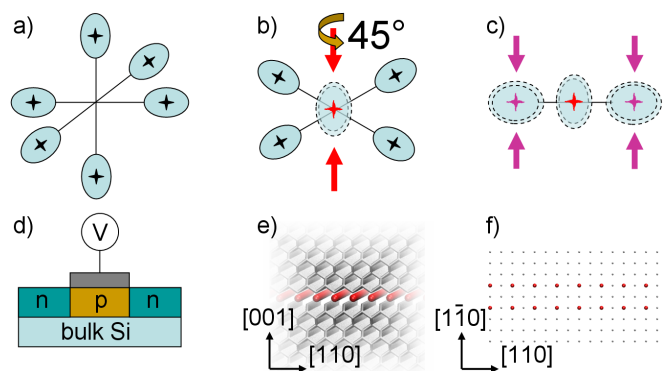


FIG. 1: Valley physics, from bulk (a), via 2D with k_z valleys collapsing (red arrows) to Γ [16–22] (b), rotating by 45° to quasi-1D confinement with $k_{x,y}$ valleys collapsing (purple arrows) onto [110] away from Γ (forming Δ valleys) (c); devices using bulk physics (d), 2D (e), and quasi-1D confinement (f).

width. This dictates much of the device behavior and scaling. Also of major interest are the Fermi level and bandstructure, especially with respect to the number of conducting modes, and the utility of the typical EMT valley picture (see Fig. 1). All of these can be gleaned from *ab initio* calculations, although the supercell sizes required to adequately describe the electronic width are formidable. *Ab initio* work also provides information guiding the progress of higher-level effective treatments such as the scTB method, or EMT.

The difficulty in describing one-dimensional structures within the supercell approximation is that the supercell must be correspondingly large in two dimensions, rather than the one dimension sufficient for δ -doped layers [20, 22, 23]. The combination of a quadratic increase in the number of atoms being considered with size and the usual N^3 scaling of density functional theory leads to a prohibitive L^6 growth in calculation time as the Si cladding (L) is increased about the wires. Using an efficient localized double- ζ with polarization (DZP) basis

set previously benchmarked against a plane-wave technique [23], it is finally possible to rigorously describe these large structures and obtain quantitative values for various properties of these nanowires.

Here we use the *ab initio* method of [24] to model two-donor-wide nanowires of monolayer-doped phosphorus in silicon, such as those of [10]. Using methodology developed to describe infinite monolayer δ -layers [22, 23], we calculate the properties of wires with 5.5 nm of silicon separating periodic images (see Supp. Mat.). We use bandstructures to find energy differences between occupied levels in the gap, including the valley splitting of the Γ bands, which can manifest experimentally as transport spectroscopy resonance series [8]. We subsequently derive and calculate anisotropic effective masses for electrons in such wires, finding results comparable to those for bulk Si and for δ -layers. We then study the electronic extent of these wires away from the donors.

Experimental structures of this type are currently built on (001) terraces of Si, patterned along or perpendicular to the well-known [110] and $[1\bar{1}0]$ Si dimer rows [8]. Once built, they are epitaxially coated with several nm of Si, and thus the P donors, which are substitutional in the lattice, return to the usual regular atomic spacing of bulk Si (001) planes, rather than the distorted dimer row positions found at the surface. In our model, we enforce periodic boundary conditions well before the surface region, therefore avoiding any potential complications from surface states. The location of the P donors has previously been shown to be negligibly different from Si lattice positions [20, 22], and is treated as such here. The most common experimental doping is 1 P atom to every four lattice sites in the monatomic plane (1/4 monolayer coverage) [8, 10], and we model wires of this density.

The random nature of the experimental in-plane PH_3 adsorption can lead to several dopant arrangements. The condition that four mutually adjacent sites be vacant means that, as in [10], a strip at least four Si-H bonds wide must be de-masked for a two-donor-wide wire to form. The regular case is one possible outcome of doping such a strip. Others include the staggered layout considered in [10], and also similar positioning with the separation increased by one atomic site. In each case, the use of periodic boundary conditions dictate that these are perfectly ordered along the wire once the transverse geometry is selected, and extension to consider disorder in this direction is utterly intractable with today's *ab initio* methods. Here, we briefly consider the staggered case for direct comparison to [10], and proceed to a detailed analysis of the regular nanowire which is more similar to the 2D δ layers considered in [20–22].

40-monolayer (ML) silicon supercells $6.17 \times 5.46 \times 0.77 \text{ nm}^3$ are presented here. P donors were substituted in positions as shown in Fig. 2, 0.86 nm (diagonally) apart in the staggered arrangement, or 0.77 nm apart in the regular 1/4 ML coverage [20–23]. The cells were designed

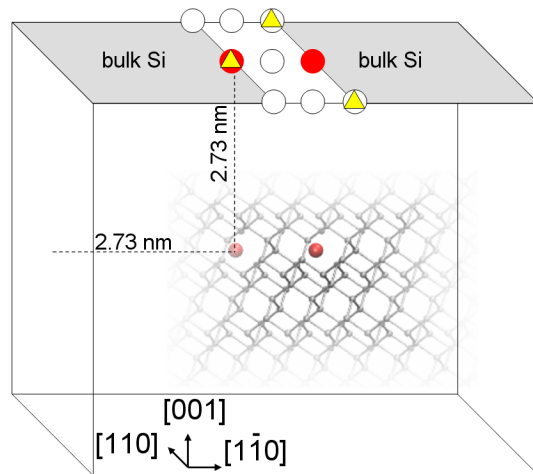


FIG. 2: (Color online) Placement of dopants in a 40 ML cell and on the top (001) face; P donor positions in staggered (yellow triangle) and regular (red circle) arrangements, Si atoms coplanar with the dopants (white circles), surrounding bulk Si (grey shaded area), periodic boundaries (solid lines).

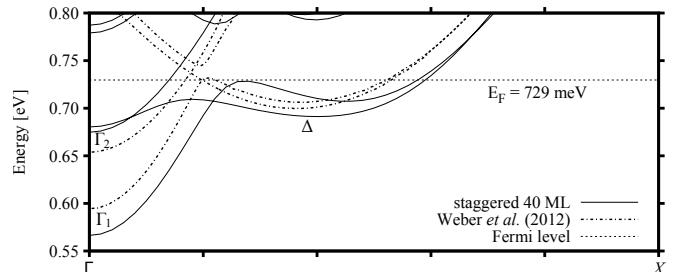


FIG. 3: Bandstructure of staggered nanowire in a 40 ML cell, by DFT and scTB (graphically estimated from [10]) with DFT energy zero set to the VBM and scTB results aligned at the Fermi level. The bandstructures run to the orthorhombic Brillouin zone X point at $1/\sqrt{8} 2\pi/a$ in the [110] k -direction.

to provide as similar an amount of cladding about the P as possible, and represent the smallest possible repeating units for 1/4 ML P distribution along the wire.

The bandstructure of the staggered wires is presented in Fig. 3. The scTB equivalent, graphically estimated from [10], is also shown, mirrored at BZ boundaries due to the longer scTB supercell (spurious bands replicated by boundary conditions have been removed). These agree qualitatively for the two lowest bands (Γ_1 and Γ_2). The third occupied band (Δ) shows qualitative agreement to the right of its crossing with Γ_1 , though there is a discrepancy inside this location. The DFT Δ band drops down to a local minimum at Γ below the Fermi level while the scTB band increases monotonically to a local maximum. This may be due to self-interaction within our calculation (intractable to correct for in such large supercells), or to an avoided crossing with the artificially low conduction band, though the general agreement is quite encouraging.

Having benchmarked our calculation against the stag-

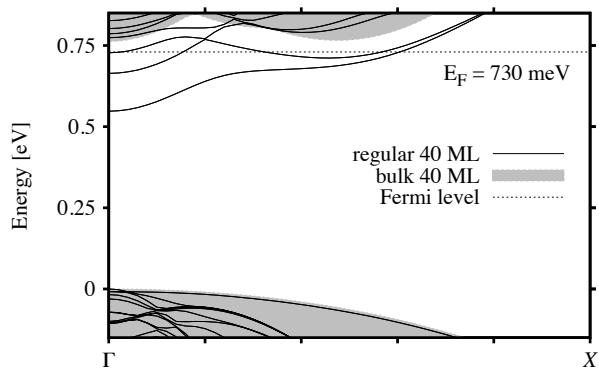


FIG. 4: Bandstructure of the regular 40 ML system.

gered case of [10] and via the methodology of [22, 23], we now proceed to study the regular case mentioned above. This is crucial, as it links to previous understanding of two-dimensional δ -layer physics [17, 20–23]. We find that the energy separations of the band minima are well-converged (to within 5 meV), in line with [22]. The bandstructure is displayed in Fig. 4, plotted from Γ to X corresponding to the wire axis. Comparison with Fig. 3 highlights disorder-related effects due to changes to the doping pattern. Due to the orthorhombic nature of the supercell, no other simple comparisons can be made to the standard FCC bandstructure. The lowered symmetry of our cell suggests two other paths with symmetry higher than one; namely from Γ to Y or Z . Bands in those directions are subject to extreme band folding (see Appendix of [22]) and are not included here.

Three bands dip below the Fermi level; the lower two have clear minima at Γ , and while the third displays a minimum in the $[110]$ direction, it also has a local minimum at Γ which dips slightly below E_F . The $[110]$ minimum will of course have a symmetric pair valley in the $[\bar{1}\bar{1}0]$ direction. We therefore predict four channels to be open for conduction along the wire. Unlike the staggered case discussed above, the Γ_1 band does not display a second minimum in the Δ direction.

The energy splittings between the bands are an important link to observable effects, as they may give rise to splittings seen between resonances in transport spectroscopy. As discussed in [8], energy levels both in a quantum dot, and in the wires leading to/from it, must be considered in such experiments. Here, we find the Γ_1 - Γ_2 splitting is 117 meV, Γ_1 - Δ (at the Δ minimum) is 164 meV, Γ_1 - Δ (at the Γ point) is 180 meV, and from the Γ_1 minimum to the Fermi level is 183 meV (from Fig. 4).

Similarly, conduction electrons' effective mass is another useful parameter. Here, according to EMT, we fit parabolae to band minima. The curvature a is directly related to m^* by $\hbar^2 k^2 / 2m_e m^* = a$. Again, the lower two bands behave in a fashion consistent with general expectations; as these bands are explicitly Γ bands, occurring

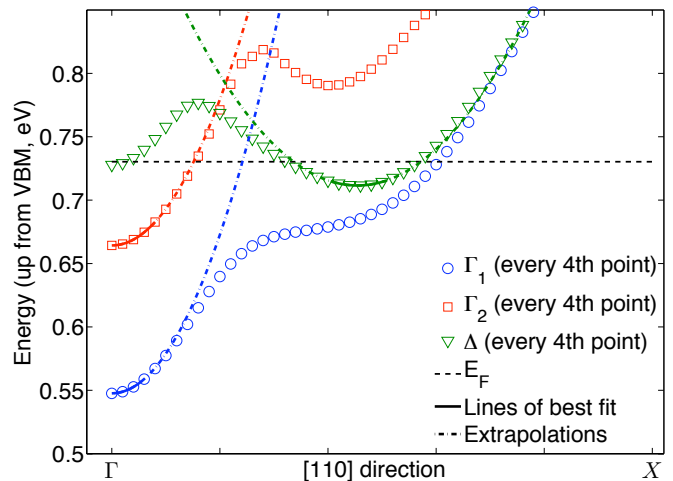


FIG. 5: (Color online) Bandstructure for regular 40 ML cell, zoomed in on states in the bandgap to fit effective masses.

as a result of z -valley projection onto Γ due to vertical confinement, we expect their physics to be governed by the transverse effective mass $m_t \sim 0.21$ [17]. Figure 5 shows DFT-generated band minima and corresponding least-squares parabolic fit curves (fit by truncating at increasing numbers of points until $|1 - \chi_r^2|$, and hence the standard error, were minimized). Agreement is very good, with χ_r^2 values of over 0.93 for points near the minima. Analysis of the curvature of the first band gives $m_t = 0.200 \pm 0.001$, falling in between the δ -layer PWO results of [17], and the experimental bulk Si value of 0.1905. The second band gives $m_t = 0.219 \pm 0.001$, which is slightly heavier than [17] suggests for δ -layers, but is likely similar enough to the first band that EMT treatments, for example, need not distinguish between them.

The x - and y -valleys, which also occur in the $\{100\}$ directions, are projected onto the $[110]$ axis due to the horizontal confinement (along $x=y$; see Fig. 1). This projection leads to a $1/\sqrt{2}$ contraction of the valley as we see it, or an effective doubling of its curvature. Reversing this projection effect leads to an estimate of the longitudinal effective mass of 0.931 ± 0.019 , in agreement with the bulk Si experimental value (0.9163) and with [17] (0.95). The parabolic fit has a χ_r^2 value of over 0.91.

Knowledge of the anisotropic effective mass is essential for longer-scale modeling techniques such as effective mass theory, or tight-binding procedures, which rely on it as a pivotal input to multiscale calculations which are more capable of describing actual devices. We can now confirm that, despite the effects of extreme confinement, the parabolic assumption holds, and that the effective masses are close enough to bulk values to be included in these techniques without modification.

To assess the electronic cross-section of the wire, we integrated the local density of states between the valence band maximum and E_F . For display purposes, we aver-

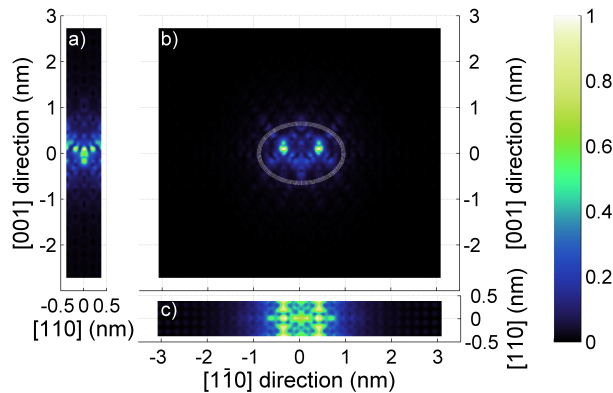


FIG. 6: (Color online) False-color representation of the electronic extent of a regular two-atom epitaxial $[110]$ Si:P nanowire in a 40 ML cell. Integrated local density of states profiles, averaged along (a) $[1\bar{1}0]$, (b) $[110]$, and (c) $[001]$, are shown, normalized to their highest values. The white ellipse is a simple two-parameter description of the region within which the wavefunction modulus exceeds $1/e$ of the maximum attributed to one Si-P bond. A color scale is also shown.

aged along the $[1\bar{1}0]$ (Fig. 6a), $[110]$ (Fig. 6b), and $[001]$ directions (Fig. 6c). The density is primarily found near the donors, in the bonds between them and the surrounding Si. The especial height of the two peaks in Fig. 6b is due to the alignment of two bonds from each P atom along the averaging direction. We therefore take 50% of the actual peak value as representative of the peak density corresponding to one Si-P bond.

A simple two-parameter model has been constructed and empirically fit to the wavefunction modulus falloff (see Supp. Mat. for more details):

$$\begin{aligned} Y_N &= (Nr + D/2)\cos(\theta), \\ Z_N &= gNr \sin(\theta), \end{aligned} \quad (1)$$

where N is the number of $1/e$ factors of falloff from the maximum value, D is the separation of the two donors (~ 0.77 nm), and r and g are parameters corresponding to a radius (0.55 nm) and a vertical scaling factor (1.20). The $N=1$ fit shown in Fig. 6b is smaller than that of [10], with a cross-section of 1.88 nm², and density fluctuations are less than 1% of the bond peak value by ± 2.0 nm along $[1\bar{1}0]$ and ± 1.5 nm along $[001]$. The extra width is due to the donor separation across the wire. The electron density is very slightly biased towards the center of the wire, and is easily explained by the presence of the second donor.

Figure 7 shows the electronic density of states evaluated over the full Brillouin zone. The valence band can be seen at left, dropping away to the bandgap (zero density). The bulk conduction band is at the extreme right. In between, we see the electronic density of states of the three occupied bands in the gap. We have a clear prediction that the wire should be conducting, as there is no

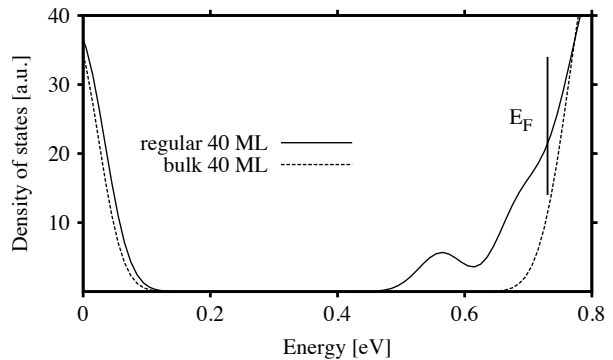


FIG. 7: Electronic density of states of a regular 40 ML cell. 50 meV Gaussian smearing has been applied for visualisation.

zero-density region near the Fermi level.

We have performed the first *ab initio* calculations of Si: δ P nanowires atomically confined both vertically and laterally, for staggered and regular layouts, observing disorder-related changes to the bandstructure. The wires are two donors wide by one high, specially placed to ensure a doping density of $1/4$ ML. The P ionic cores provide extreme confinement in anisotropic fashion due to their placement. Qualitative agreement with the recent staggered pattern scTB results of [10] is encouraging, supporting their new multiscale technique which can handle larger device volumes. Bandstructure and Fermi-level analysis show considerable donor placement effects, and leads us to predict four open conduction channels; two each governed by the transverse and longitudinal effective masses, which have been calculated and matched explicitly to bulk values – essentially linking classical device understanding to these novel single-atom defined nanoelectronic devices and their function, and confirming the utility of the effective mass approximation on these atomic scales. Further, approaches which explicitly assume these values as inputs (EMT, TB) now have validation for this axiom. Connection to previous *ab initio* models with one dimension of confinement is made via the regular model, and is thoroughly explored, including the development of a simple two-parameter model describing the falloff of the wavefunction modulus.

Acknowledgements

The authors thank J.H. Cole for discussions, and acknowledge funding by the ARC Discovery grant DP0986635. This research was undertaken on the NCI National Facility, Canberra, Australia.

* Electronic address: d.drumm@student.unimelb.edu.au

- [1] J. R. Tucker and T.-C. Shen. *Solid-State Electron.*, 42:1061, 1998.
- [2] J. L. O'Brien, S. R. Schofield, M. Y. Simmons, R. G. Clark, A. S. Dzurak, N. J. Curson, B. E. Kane, N. S. McAlpine, M. E. Hawley, and G. W. Brown. *Phys. Rev. B*, 64:161401(R), 2001.
- [3] T.-C. Shen, J.-Y. Ji, M. A. Zudov, R.-R. Du, J. S. Kline, and J. R. Tucker. *Appl. Phys. Lett.*, 80:1580, 2002.
- [4] T.-C. Shen, J. S. Kline, T. Schenkel, S. J. Robinson, J.-Y. Ji, C. Yang, R.-R. Du, and J. R. Tucker. *J. Vac. Sci. Technol. B*, 22:3182, 2004.
- [5] F. J. Ruess, L. Oberbeck, K. E. J. Goh, M. J. Butcher, E. Gauja, A. R. Hamilton, and M. Y. Simmons. *Nanotechnology*, 16:2446, 2005.
- [6] F. J. Ruess, W. Pok, T. C. G. Reusch, M. J. Butcher, K. E. J. Goh, L. Oberbeck, G. Scappucci, A. R. Hamilton, and M. Y. Simmons. *Small*, 3:563, 2007.
- [7] F. J. Ruess, K. E. J. Goh, M. J. Butcher, T. C. G. Reusch, L. Oberbeck, B. Weber, A. R. Hamilton, and M. Y. Simmons. *Nanotechnology*, 18:044023, 2007.
- [8] M. Fuechsle, S. Mahapatra, F. A. Zwanenburg, M. Friesen, M. A. Eriksson, and M. Y. Simmons. *Nature Nanotechnology*, 5:502, 2010.
- [9] M. Fuechsle, J. A. Miwa, S. Mahapatra, H. Ryu, S. Lee, O. Warschkow, L. C. L. Hollenberg, G. Klimeck, and M. Y. Simmons. *Nature Nanotechnology*, 7:242, 2012.
- [10] B. Weber, S. Mahapatra, H. Ryu, S. Lee, A. Fuhrer, T. C. G. Reusch, D. L. Thompson, W. C. T Lee, G. Klimeck, L. C. L. Hollenberg, and M. Y. Simmons. *Science*, 335:64, 2012.
- [11] A. Fert. *Rev. Mod. Phys.*, 80:1517, 2008.
- [12] D. Culcer, X. Hu, and S. Das Sarma. *Appl. Phys. Lett.*, 95:073102, 2009.
- [13] B. E. Kane. *Nature*, 393:133, 1998.
- [14] D. Loss and D. P. DiVincenzo. *Phys. Rev. A*, 57:120, 1998.
- [15] L. C. L. Hollenberg, A. S. Dzurak, C. Wellard, A. R. Hamilton, D. J. Reilly, G. J. Milburn, and R. G. Clark. *Phys. Rev. B*, 69:113301, 2004.
- [16] D. W. Drumm, L. C. L. Hollenberg, M. Y. Simmons, and M. Friesen. *Phys. Rev. B*, 85:155419, 2012.
- [17] G. Qian, Y.-C. Chang, and J. R. Tucker. *Phys. Rev. B*, 71:045309, 2005.
- [18] H. Ryu, S. Lee, and G. Klimeck. A study of temperature-dependent properties of n-type δ -doped si band-structures in equilibrium. *IEEE proceedings of the 13th International Workshop on Computational Electronics*, 2009; arXiv:1003.4926v1 [cond-mat.mtrl-sci], 2009.
- [19] H. Ryu, S. Lee, B. Weber, S. Mahapatra, M. Y. Simmons, L. C. L. Hollenberg, and G. Klimeck. Quantum transport in ultra-scaled phosphorus-doped silicon nanowires. In *Silicon Nanoelectronics Workshop 2010*, pages 1–2, 2010.
- [20] D. J. Carter, O. Warschkow, N. A. Marks, and D. R. McKenzie. *Phys. Rev. B*, 79:033204, 2009.
- [21] D. J. Carter, N. A. Marks, O. Warschkow, and D. R. McKenzie. *Nanotechnology*, 22:065701, 2011.
- [22] D. W. Drumm, A. Budi, M. C. Per, S. P. Russo, and L. C. L. Hollenberg. *Nanoscale Research Letters*, 2013 (in press). arXiv:1201.3751 [cond-mat.mtrl-sci], 2012.
- [23] A. Budi, D. W. Drumm, M. C. Per, A. Tregonning, S. P. Russo, and L. C. L. Hollenberg. *Phys. Rev. B*, 86:165123, 2012.
- [24] E. Artacho, E. Anglada, O. Diéguez, J. D. Gale, A. García, J. Junquera, R. M. Martín, P. Ordejón, J. M. Pruneda, D. Sánchez-Portal, and J. M. Soler. *J. Phys.: Condensed Matter*, 20:064208, 2008.